

0017-9310(94)E0032-P

# Numerical study of turbulent flow in two-dimensional channel with surface mounted obstacle

YUE-TZU YANG and SHIARNG YANG

National Cheng Kung University Tainan, Taiwan 701, China

(Received 5 December 1993)

**Abstract**—This paper presents the numerical predictions of the fluid and heat transfer characteristics for the turbulent channel flow with one and two obstacles. The turbulent governing equations are solved by a control-volume-based finite-difference method with non-uniform staggered grids and the well-known  $k-\epsilon$  model and its associated wall function to describe the turbulence structure. The velocity and pressure terms of momentum equations are solved by the SIMPLE method. The parameters interested include entrance Reynolds number (between  $10^4$  and  $10^6$ ), the ratio of channel height to obstacle height ( $B/H$ ) and the dimensionless distance between two obstacles ( $PR$ ). Computations are carried out for three working mediums, air, water and Freon R-12. The predicted attachment point located at  $x/H = 12.24$  are compared with the experimental results of  $x/H = 12.3$  for the unheated single obstacle case with  $B/H = 15$ . The predicted heat transfer around the attachment point is much better than that in the recirculation region due to the strong impact at the attachment point.

## INTRODUCTION

Turbulent flow around bluff bodies forms an important group of separated flows occurring in many situations of practical interest. It is difficult to predict this flow field since it poses many problems for numerical methods and turbulence models because of the curved streamlines and steep velocity/pressure gradients surrounding the body. The present investigation is concerned with the prediction of the particular case of turbulent flow around two-dimensional surface-mounted obstacles.

In engineering applications, the turbulent flow in a channel with surface-mounted obstacles become more important. For example, the volume of electric device becomes very small, the arrangement and the cooling system of the electric device can not be ignored. So, the first step of designing electric circuit must depend on the characteristic of heat transfer. Otherwise, this flow field also can use these obstacles to increase the disturbance, these obstacles can increase the efficiency of heat transfer and the total efficiency of the heat exchanger. So far, many investigators have considered the similar flow field. But few are focusing on the turbulent flow field and the performance of heat transfer or with two obstacles on one surface in a channel. In fact, such a flow field combine several basic flow fields. It includes channel flow, forward facing step flow, backward facing step flow and even cavity flow and so on. This flow field contains flow separation, reattachment, redeveloping flow along the wall and developed flow. Wirtz and McAuliffe [1] described the

obstacles as a large electric device and the bottom surface behind the obstacles as many small dense IC, as shown in Fig. 1.

The channel flow with surface-mounted obstacles is so complex that most investigations have been confined to experimental analysis [2–4]. The parameters include entrance Reynolds number (characteristic length is two times channel height) and the ratio of channel height to obstacle height ( $B/H$ ). Crabb *et al.* [2] studied the flow field of  $B/H = 15$ , Rastogi *et al.* [3] analysed the experiment of  $B/H = 2$ , and Castro *et al.* [4] studied the experiments of  $B/H = 5, 8, 15$  and  $20$  with  $Re = 10^4$ – $10^6$ . The effect of heat transfer was not considered in their studies.

As computer executing speed becomes faster and faster, many scholars tend to use a variant scheme and a procedure to discrete the equation of motion. For example, Benodekar *et al.* [5] used the PISO (Pressure-Implicit-Split-Operator) method to calculate such a flow field and compare their results with the experimental results of Crabb and Durao [2]. Zebib and Wo [6] investigated the flow field in which the obstacles are heated (keeping constant temperature or constant heat flux), but the flow is considered as laminar not turbulent. Kim *et al.* [7] considered periodical obstacles to calculate the laminar flow field. Recently, Liou *et al.* [8], however, considered turbulent flow to analyse such problems.

According to the suggestion of Wirtz and McAuliffe [1], it is necessary to use turbulent flow to cool the electric device system in the future. So, it is important to know the details of such a flow field.

## NOMENCLATURE

$B$	channel height	Greek symbols	
$C_1, C_2, C_\mu$	turbulent constant	$\alpha$	thermal diffusivity
$C_p$	pressure coefficient	$\delta$	boundary thickness
$H$	obstacle height	$\epsilon$	turbulent energy dissipation rate
$h$	heat transfer coefficient	$\kappa$	Von Karman constant
$i$	turbulence intensity	$\mu$	dynamic viscosity
$k$	turbulent kinetic energy	$\nu$	kinematic viscosity
$P$	pressure	$\rho$	density
$PR$	obstacle-pitch to obstacle-height	$\sigma$	turbulent Prandtl number
$Pr$	Prandtl number	$\tau$	shear stress.
$q''$	heat flux	Subscripts	
$Re$	Reynolds number	in	inlet condition
$T$	temperature	eff	effective
$U_o$	free stream (inlet) velocity	l	laminar
$u$	$x$ -component velocity	t	turbulent
$v$	$y$ -component velocity	w	wall.
$Xr$	reattachment point		
$x$	$x$ coordinate		
$y$	$y$ coordinate.		

## MATHEMATICAL FORMULATION

## Governing equation

The flow under consideration is governed by the two-dimensional form of the continuity and the time-averaged Navier-Stokes equations. In a Cartesian coordinate system for steady-state, incompressible flow, neglecting buoyancy, these equations can be written in the following general form:

$$\frac{\partial}{\partial x}(\rho u \phi) + \frac{\partial}{\partial y}(\rho v \phi) = \frac{\partial}{\partial x} \left[ \Gamma_\phi \frac{\partial \phi}{\partial x} \right] + \frac{\partial}{\partial y} \left[ \Gamma_\phi \frac{\partial \phi}{\partial y} \right] + S_\phi, \quad (1)$$

where  $\phi$  stands for the dependent variables  $u, v, k, \epsilon,$  and  $T$ ;  $u$  and  $v$  are local time-averaged velocity in

$x$  and  $y$  directions, respectively;  $\Gamma_\phi$  and  $S_\phi$  are the corresponding turbulent diffusion coefficient and source term, respectively, for the general variable  $\phi$ . The equations are summarized in Table 1. The turbulent viscosity  $\mu_T$  and  $\mu_e$  can be written as:

$$\mu_T = \rho \nu_T = \rho C_\mu \frac{k^2}{\epsilon}, \quad (2)$$

$$\mu_e = \mu_l + \mu_T = \mu_l + \rho C_\mu \frac{k^2}{\epsilon}. \quad (3)$$

The constants of the  $k$ - $\epsilon$  turbulence model suggested by Launder and Spalding [9] are shown in Table 2.

## Boundary conditions

The computational domain boundaries are shown in Fig. 2, with a non-uniform staggered grid system which finer grids near the wall.

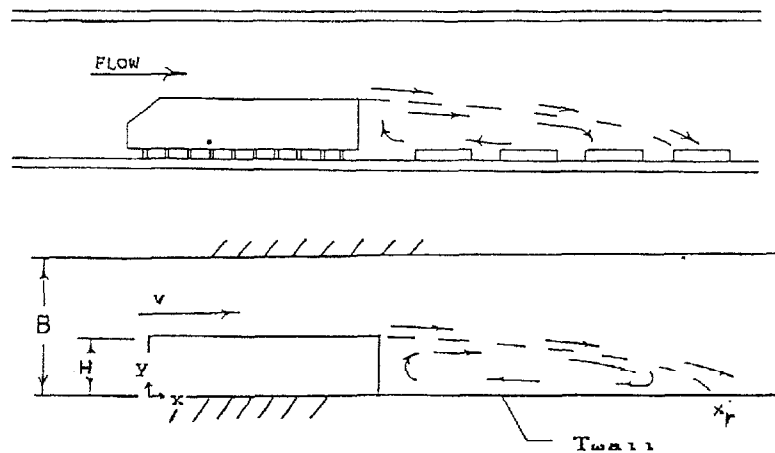


Fig. 1. Schematic of flow for engineering application and computational model.

Table 1. Conservation equations

Equation	$\phi$	$\Gamma_\phi$	$S_\phi$
Mass	1	0	0
X-momentum	$u$	$\mu_e$	$-\frac{\partial p}{\partial x} + \frac{\partial}{\partial x} \left( \mu_e \frac{\partial u}{\partial x} \right) + \frac{\partial}{\partial y} \left( \mu_e \frac{\partial v}{\partial x} \right)$
Y-momentum	$v$	$\mu_e$	$-\frac{\partial p}{\partial y} + \frac{\partial}{\partial x} \left( \mu_e \frac{\partial u}{\partial y} \right) + \frac{\partial}{\partial y} \left( \mu_e \frac{\partial v}{\partial y} \right)$
Energy	$T$	$\frac{\mu_e}{\sigma_e}$	0
Turbulent kinetic energy	$k$	$\frac{\mu_e}{\sigma_k}$	$G - \rho \varepsilon$
Turbulent energy dissipation rate	$\varepsilon$	$\frac{\mu_e}{\sigma_\varepsilon}$	$\frac{\varepsilon}{k} (C_1 G - C_2 \rho \varepsilon)$

where  $G = \mu_\tau \left\{ 2 \left[ \left( \frac{\partial u}{\partial x} \right)^2 + \left( \frac{\partial v}{\partial y} \right)^2 \right] + \left( \frac{\partial u}{\partial y} + \frac{\partial v}{\partial x} \right)^2 \right\}$ .

1. *Inlet boundary (AH).* At the inlet boundary, uniform flow conditions are imposed as follows:

$$U = U_{in} \quad k = k_{in} = iU_{in}^2$$

$$\varepsilon = \varepsilon_{in} = \frac{k_{in}^{1.5} C_\mu^{0.75}}{C_\mu \delta} T = T_{in}, \quad (4)$$

where  $i$  is turbulence intensity and  $\delta$  is boundary thickness.

2. *Channel walls and obstacles surfaces.* In this study,

Table 2. Constants of the  $k-\varepsilon$  model

$C_\mu$	$C_1$	$C_2$	$\sigma_k$	$\sigma_\varepsilon$	$\sigma_\tau$
0.09	1.44	1.92	1.0	1.3	0.8

the near-wall region was simulated by two zone model, i.e. viscous sublayer and fully turbulent zone, and the wall function method [10] was used to bridge the viscous sublayer. Near the corners of the obstacle the finite difference grids were treated specially, as shown in Fig. 3. The wall function approach consists of the assumption that the grid points nearest to the solid wall, that is, at a distance  $y_p$  from the nearest wall, a component parallel to the wall ( $U_p$ ) obeys the following equations:

$$\tau_w = \frac{\mu_l U_p}{y_p} \quad \text{when } y^+ < 11.63$$

$$\tau_w = \kappa \rho C_\mu^{1/4} k_p^{1/2} \frac{U_p}{\ln(Ey^+)} \quad \text{when } y^+ \geq 11.63,$$

where  $y^+ = \frac{U_\tau y_p}{\nu}$ . (5)

The assumption that at the same location the production of  $K$  is in equilibrium with the dissipation of  $\varepsilon$ . If  $k_p$  and  $\varepsilon_p$  are the  $k$  and  $\varepsilon$  at  $Y = y_p$ , then it can be shown that the conditions imposed on the  $k$  equation and  $\varepsilon$  equation instead of solid-wall boundary conditions are:

$$k_p = \frac{U_\tau^2}{C_\mu^{1/2}} \quad \varepsilon_p = C_\mu^{3/4} \frac{k_p^{3/2}}{\kappa y_p}. \quad (6)$$

In addition, the temperature distribution  $T_p$  at point  $p$  is obtained from

$$T^+ = \sigma y^+ \quad \text{when } y^+ < 11.63$$

$$T^+ = \sigma_\tau \left[ \frac{1}{K} \ln(Ey^+) + P \right] \quad \text{when } y^+ \geq 11.63,$$

where  $T^+ = \frac{T_w - T}{T^*}$

and  $T^* = \frac{\alpha q_w}{k U_\tau}$ , (7)

and Jayetilleke [11] defined the experimental  $P$  function as:

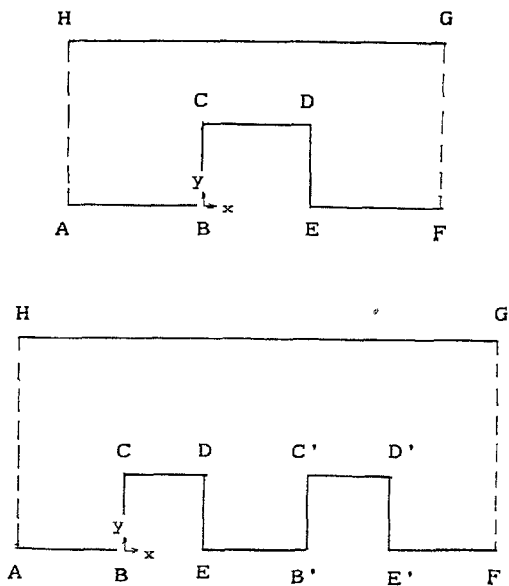


Fig. 2. Sketch of configuration and coordinate system of the calculating domain.

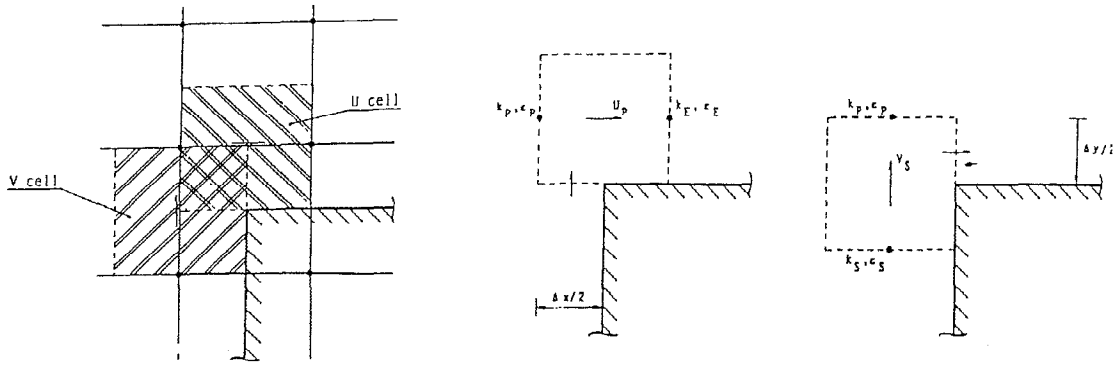


Fig. 3. Computational cells near plate corner.

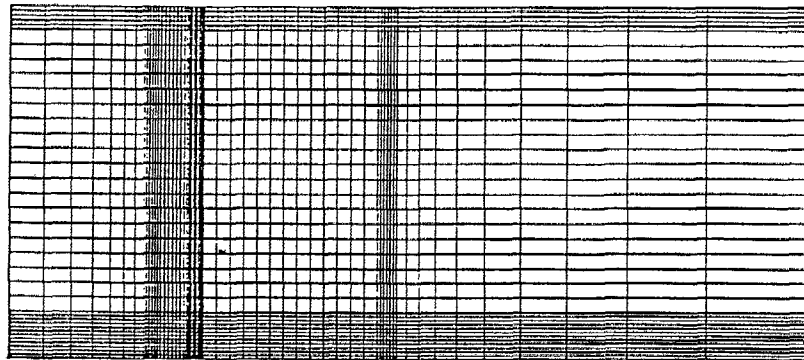


Fig. 4. Sketch of grid arrangement.

$$P = 9.24 \left\{ \left[ \left( \frac{\sigma}{\sigma_T} \right)^{0.75} - 1 \right] \times \left[ 1 + 0.28 \times \exp \left( -0.007 \times \frac{\sigma}{\sigma_T} \right) \right] \right\}$$

3. Outlet boundary.

The flow field can be regarded as fully developed when the outlet is located far away from recirculation region. Usually, the outlet is located at 25–30 times the obstacle height behind the obstacle. So, zero normal gradients at the outlet plane are given as:

$$\frac{\partial u}{\partial x} = 0 \quad \frac{\partial v}{\partial x} = 0 \quad \frac{\partial T}{\partial x} = 0. \quad (8)$$

**NUMERICAL PROCEDURE**

The numerical method used in the present study is based on the SIMPLE algorithm of Patankar and Spalding[12]. The conservation equations are discretized by a control volume based finite difference method with a power-law scheme. The set of difference equations are solved iteratively using a line by line solution method in conjunction with a tridiagonal matrix form. Based on the grid independence study, (50 × 32) is used. The solution is considered to be converged when the normalized residual of the

algebraic equation is less than a prescribed value of 0.001.

**RESULTS AND DISCUSSION**

*Effect of grid refinement*

A non-uniform grid arrangement was used in the present computations and shown in Fig. 4. The grid system was suggested with the velocity nodes displaced from scalar nodes. Grid independence test was performed with four different grid sizes, namely 36 × 22, 44 × 26, 50 × 32 and 58 × 38. And we used the calculation results of above various grid refinement to

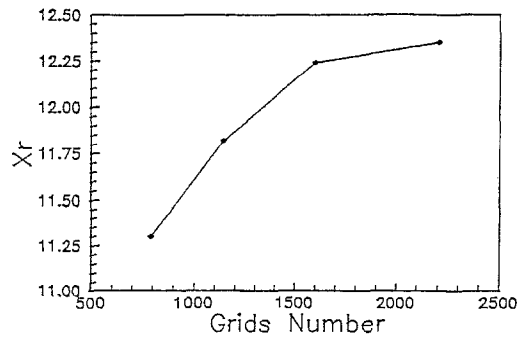


Fig. 5. Effect of grid refinement on reattachment length.

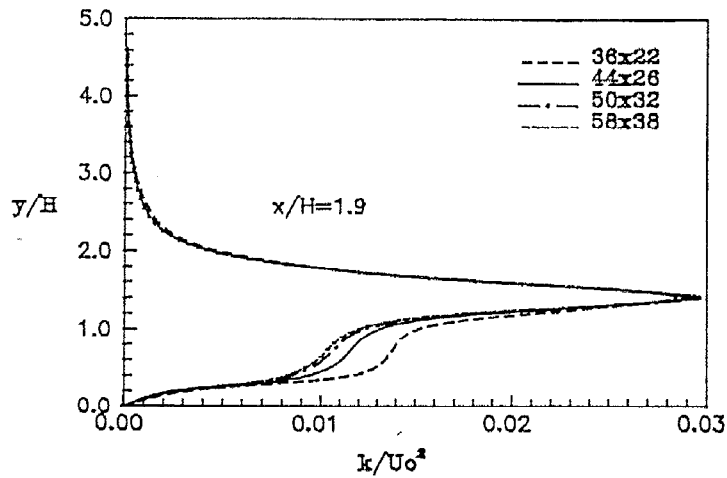


Fig. 6. Effect of grid refinement on turbulent kinetic energy.

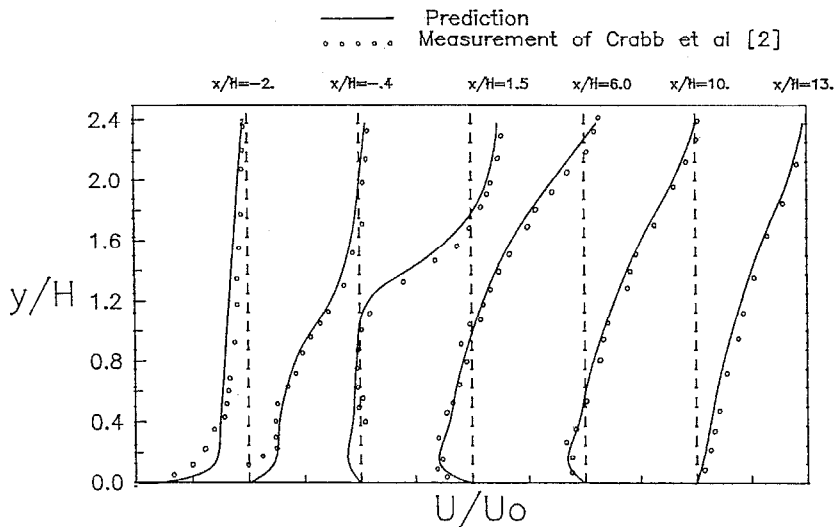


Fig. 7. Velocity predictions and measurements of Crabb *et al.* [2].

compare with the experimental results of Crabb *et al.* [2]. The parameters used to check the grid independence of the computational results were the reattachment length ( $X_r$ ), which has historically been used to assess the overall predictive capability of turbulence models, and the turbulent kinetic energy profiles, as shown in Figs. 5 and 6. The calculation solutions appear to be independent of grid distribution of  $50 \times 32$ .

We extended also the investigations to set two obstacles on the channel wall and used various working medium to predict the characteristic of flow field and performance of heat transfer.

*Predictions and comparison with experimental data*

1. *One obstacle mounted on channel wall.* The experimental results and calculation solutions have a good agreement, shown in Fig. 7. The reattachment length

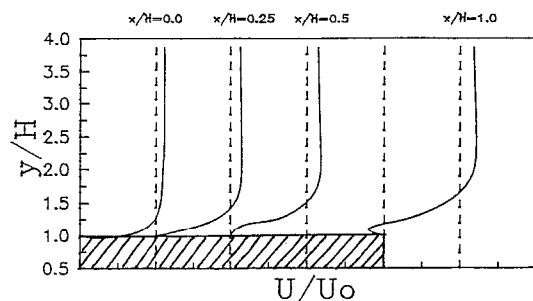


Fig. 8. Velocity predictions on top of the obstacle.

of calculation is only 0.49% shorter than that of the experimental results of Crabb *et al.* [2]. Velocity distribution above the top of obstacle has the recirculation region as shown in Fig. 8. The calculation

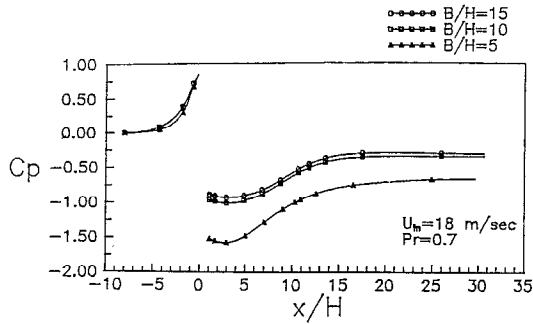


Fig. 9. Wall static pressure distribution for flow over the obstacle.

solutions compare with the experimental phenomena quite well. The predicted wall static pressure distribution is shown in Fig. 9. It is found that, behind the obstacle, the wall static pressure changes sensitively at a small aspect ratio  $B/H = 5$ .

The heated section is located at the bottom wall which is behind the obstacle. The local surface temperature  $T_w$  is kept constant, and the local heat flux along this heated surface is  $q''$ . The local heat transfer coefficient  $h$  was determined as:

$$h = \frac{q''}{T_w - T_{in}} \quad (9)$$

The flow separates at the trailing edge of the obstacle, forming a wake region downstream where the heated surface is located. Since the coolant flow is separated in the wake region, heat transfer from the obstacle is reduced relative to what would occur in the absence of the obstacle. Therefore, in the recirculation region the heat transfer is very poor, especially near the obstacle. After the reattachment point, the thermal boundary layer begins to develop, and its thickness becomes more thicker. So, behind the reattachment point, the heat transfer becomes weak. But around the reattachment point, the flow impact is very strong,

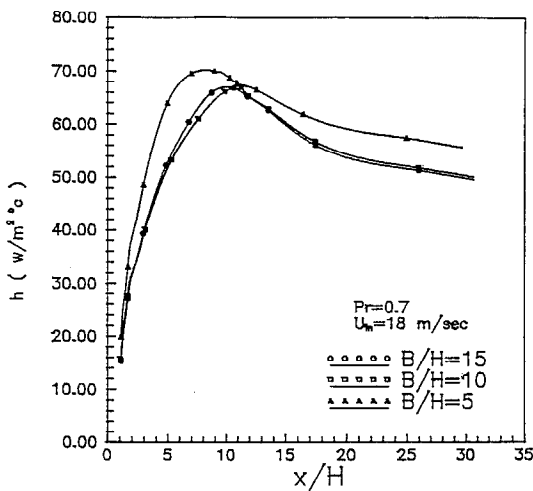
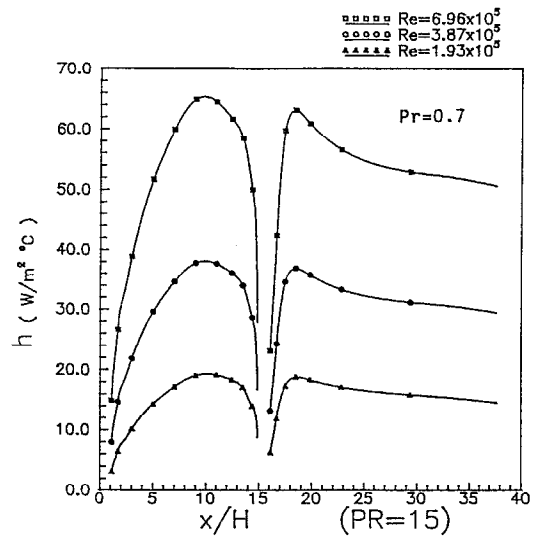
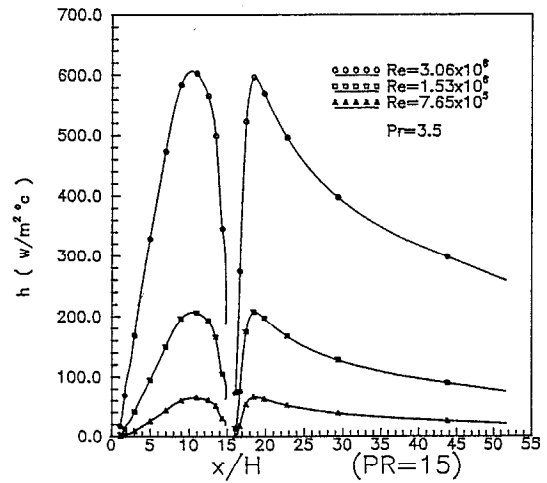


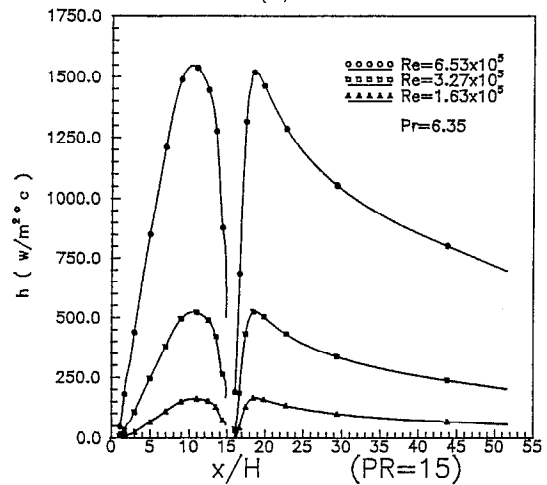
Fig. 10. Local heat transfer coefficient distribution.



(a)



(b)



(c)

Fig. 11. Local heat transfer coefficient for different working media.

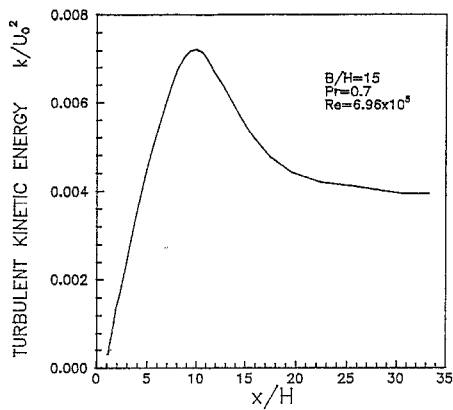


Fig. 12. Distribution of turbulent kinetic energy.

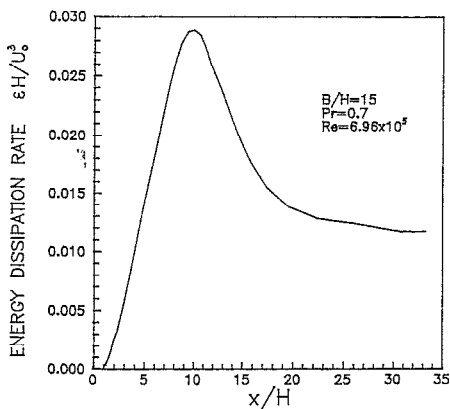


Fig. 13. Distribution of turbulent energy dissipation rate.

so the heat transfer performance is very good, as shown in Fig. 10.

2. *Two obstacles mounted on the channel wall.* The flow field with two obstacles mounted on the channel wall is a very complex flow field. It contains forward facing step flow, backward facing step flow and cavity flow. The results show that in the cavity only around the middle is the heat transfer good, and especially around the corner the heat transfer is very poor. Behind the second obstacle, the phenomenon is as same as with only one obstacle. The heat transfer coefficient decreased rapidly after the second obstacle if water or Freon R-12 is used as a working medium, as shown in Fig. 11.

At the top of the obstacles, we can also find a recirculation region that consists of physical phenomena. In Fig. 12, it appears that the highest turbulence kinetic energy  $k$  is located around the attachment point. The result is due to a high impact at the attachment point. The same phenomena can be seen in the distribution of the turbulence energy dissipation rate  $\epsilon$ , shown in Fig. 13, and this is due to a great velocity gradient.

## CONCLUSIONS

As the volume of IC becomes smaller in the future, the cooling system will become more important. So, it is necessary to use a turbulent flow field to cool the electric device system. Beside using various flow patterns, in order to increase the performance of heat transfer, we can use various mediums as a coolant. According to the characteristics of the heat transfer coefficient, we can design the electric device system effectively, and as dense as possible. So, it is necessary to understand the characteristic of the heat transfer when we use various flow patterns or various working mediums in an electric cooling system.

## REFERENCES

1. R. A. Wirtz and W. McAuliffe, Experimental modeling of convection downstream from an electronic package row, *J. Electron. Packing* **111**, 207–212 (1989).
2. D. Crabb, D. F. G. Durao and J. H. Whitelaw, Velocity characteristics in the vicinity of a two dimensional rib, *Proceedings of the 4th Brazilian Congress on Mechanical Engineering*, Florianopolis, Brazil, pp. 415–429 (December 1977).
3. F. Durst and A. K. Rastogi, Theoretical and experimental investigations of turbulent flows with separation. In *Turbulent Shear Flow I* (Edited by F. Durst, B. E. Launder, F. W. Schmidt and J. H. Whitelaw), pp. 208–219 (1979).
4. I. P. Castro and J. E. Fackrell, A note on two-dimensional fence flows with emphasis on wall constraint, CEGB (MEL) Report (Southampton, Hampshire, U.K.).
5. R. W. Benodekar, A. J. H. Goddard, A. D. Gosman and R. I. Issa, Numerical prediction of turbulent flow over surface-mounted ribs, *AIAA J.* **23**, 359–365 (1985).
6. A. Zebib and Y. K. Wo, A two-dimensional conjugate heat transfer model for forced air cooling of an electronic device, *J. Electron. Packing* **111**, pp. 41–45 (1989).
7. S. H. Kim and N. K. Anand, Periodically fully developed flow in channels with conducting blockages, *J. Thermophysics* **6**, 91–97.
8. T. M. Liou, J. J. Hwang and S. H. Chen, Turbulent transport phenomena in a channel with periodic rib turbulators, *J. Thermophys. Heat Transfer* **6**, 513–521 (1992).
9. B. E. Launder and D. B. Spalding, *Mathematical Models of Turbulence*, Chapter 5, pp. 90–110. Academic Press, London (1972).
10. N. Djilali, I. Gartshore and M. Salcudean, Calculation of convective heat transfer in recirculation turbulent flow using various near-wall turbulence models, *Numer. Heat Transfer* **16** (1989).
11. C. L. V. Jayatilake, The influence of Prandtl number and surface roughness on the resistance of the laminar sublayer to momentum and heat transfer, *Prog. Heat Mass Transfer* **1**, 193–329 (1969).
12. S. V. Patankar, *Numerical Heat Transfer and Fluid Flow*, Chapters 5 and 6, pp. 79–138. McGraw-Hill, New York (1980).
13. R. Subhashis and J. Srinivasan, Analysis of conjugate laminar mixed convection in a shrouded array of electronic components, *Int. J. Heat Mass Transfer* **35**, 815–822 (1992).